Combined Car−Parrinello QM/MM Dynamic Study on the Propagation and Termination Steps of Ethylene Polymerization Catalyzed by [$Cp_2ZrR(\mu$-Me)$B(C_6F_5)_3$] (R = Me, Pr)

Sheng-Yong Yang and Tom Ziegler*

Department of Chemistry, University of Calgary, University Drive 2500, Calgary, Alberta, Canada T2N 1N4

Received September 29, 2005

Combined Car−Parrinello and QM/MM dynamic simulations have been carried out in order to investigate the polymer chain propagation and termination processes in ethylene polymerization catalyzed by zirconocene with the counteranion $[CH_3B(C_6F_5)_3]^-$ included. A complete account is given not only of the potential energy profile (PEP) but also of the free energy profile (FEP) for the first and second steps of ethylene insertion, as well as of the chain termination. Solvation effects were included on the basis of a continuum model. Special attention was given to the counteranion mobility in the catalytic process and the possible differences between PEP and FEP. Two different modes of attack by ethylene, *cis* and *trans* to the counteranion $[CH_3B(C_6F_5)_3]^-$, were considered. In general, the FEPs differ from the PEPs in the barrier height and the shape. The FEP gives a higher barrier over PEP due to entropic contributions. The transition state of ethylene uptake by the metal center, the ethylene π-complex, and the ethylene insertion transition state are all clearly present on the FEPs. This is not always the case for the PEPs, especially for the *trans* pathway. The calculated FEPs for the chain propagation indicate that the *cis* pathway is preferred over the *trans* pathway for both the first and second insertions. For the energetically favorable *cis* pathway, the ethylene insertion into the $Zr-C_\alpha$ bond rather than the ethylene uptake by the metal center is the rate-determining step for both PEP and FEP (with/without solvation effects included). Free dynamic simulations without any constraint on the process after ethylene insertion show that the counteranion can recoordinate to the metal center again in a period of less than 1 ps. In comparison with the estimated time scale of the chain propagation, the counteranion which was displaced by ethylene in the ethylene uptake process has sufficient time to recombine with $[Cp_2ZrR]^+$ again before a new monomer approaches to the metal center. This is in good agreement with very recent experiments. The energetically most favorable pathway for the chain termination corresponds to the *cis* approach, with a free energy barrier of 18.5 kcal/mol.

1. Introduction

Single-site homogeneous catalysts containing a group IV transition metal have attracted considerable attention both experimentally and theoretically over the past two decades.[1] This interest stems from the expectation that they at least in part might replace the classical Ziegler−Natta catalysts. Of special interest are zirconocenes and their derivatives, due to the high activities of these compounds.[1] Zirconocenes of the type Cp_2ZrMe_2 are not very effective as polymerization catalysts without activation by a Lewis acid (A), such as $B(C_6F_5)_3$. In the activation process A will extract one of the methyl groups to produce the ion pair $[Cp_2ZrMe]^+[MeA]^-$ (Scheme 1a). It has further been established that the cation $[Cp_2ZrMe]^+$ is the active species in the polymerization process.[2] On the basis of this information, early theoretical studies would focus on the cation part $[Cp_2ZrMe]^+$ [3−7] and for the most part ignore the counteranion.

Marks et al.[1b] were the first to demonstrate from a computational study on $[H_2Si(C_5H_4)(^tBuN)Ti(CH_3)]^+[CH_3B(C_6H_5)_3]^-$ that the counteranion can significantly affect the catalyst performance during olefin polymerization. This conclusion has been further corroborated in subsequent studies by Lanza,[8] Fusco,[9] Nifant'ev,[10] Ziegler,[11] and others[12] on the basis of

* To whom correspondence should be addressed. E-mail: ziegler@ucalgary.ca.

(1) For recent reviews, see: (a) Bochmann, M. *J. Organomet. Chem.* **2004**, *689*, 3982. (b) Chen, E. Y.-X.; Marks, T. J. *Chem. Rev.* **2000**, *100*, 1391. (c) Kaminsky, W. *Metalorganic Catalysts for Synthesis and Polymerization: Recent Results by Ziegler−Natta and Metallocene Investigations*; Springer-Verlag: Berlin, 1999. (d) Britovsek, G. J. P.; Gibson, V. C.; Wass, D. F. *Angew. Chem., Int. Ed.* **1999**, *38*, 428. (e) Jordan, R. F. *J. Mol. Catal.* **1998**, *128*, 1. (f) McKnight, A. L.; Waymouth, R. M. *Chem. Rev.* **1998**, *98*, 2587. (g) Kaminsky, W.; Arndt, M. *Adv. Polym. Sci.* **1997**, *127*, 144. (h) Bochmann, M. *J. Chem. Soc., Dalton Trans.* **1996**, *255*. (i) Brintzinger, H. H.; Fischer, D.; Mülhaupt, R.; Rieger, B.; Waymouth, R. M. *Angew. Chem., Int. Ed. Engl.* **1995**, *34*, 1143.

(2) (a) Jordan, R. F. *J. Chem. Educ.* **1988**, *65*, 285. (b) Ewen, J. A. *J. Am. Chem. Soc.* **1984**, *106*, 6355.

(3) Jolly, C. A.; Marynick, D. S. *J. Am. Chem. Soc.* **1989**, *111*, 7968.

(4) (a) Yoshida, T.; Loga, N.; Morokuma, K. *Organometallics* **1995**, *14*, 746. (b) Kawamura-Kuribayashi, H.; Loga, N.; Morokuma, K. *J. Am. Chem. Soc.* **1992**, *114*, 8687. (c) Vyboishchikov, S. F.; Musaev, D. G.; Froese, R. D. J.; Morokuma, K. *Organometallics* **2001**, *20*, 309.

(5) Fusco, R.; Longo, L.; Masi, F.; Garbassi, F. *Macromolecules* **1997**, *30*, 7673.

(6) (a) Lohrenz, J. C. W.; Woo, T. K.; Ziegler, T. *J. Am. Chem. Soc.* **1995**, *117*, 2793. (b) Woo, T. K.; Fan, L.; Ziegler, T. *Organometallics* **1994**, *13*, 2252. (c) Lohrenz, J. C. W.; Woo, T. K.; Fan, L.; Ziegler, T. *J. Organomet. Chem.* **1995**, *497*, 91. (d) Margl, P.; Deng, L.; Ziegler, T. *Organometallics* **1998**, *17*, 933.

(7) Lanza, G.; Fragalà, I. L.; Marks, T. J. *J. Am. Chem. Soc.* **2000**, *122*, 12764.

(8) Lanza, G.; Fragalà, I. L.; Marks, T. J. *J. Am. Chem. Soc.* **1998**, *120*, 8257.

10.1021/om050840s CCC: $33.50
Publication on Web 01/10/2006

Scheme 1

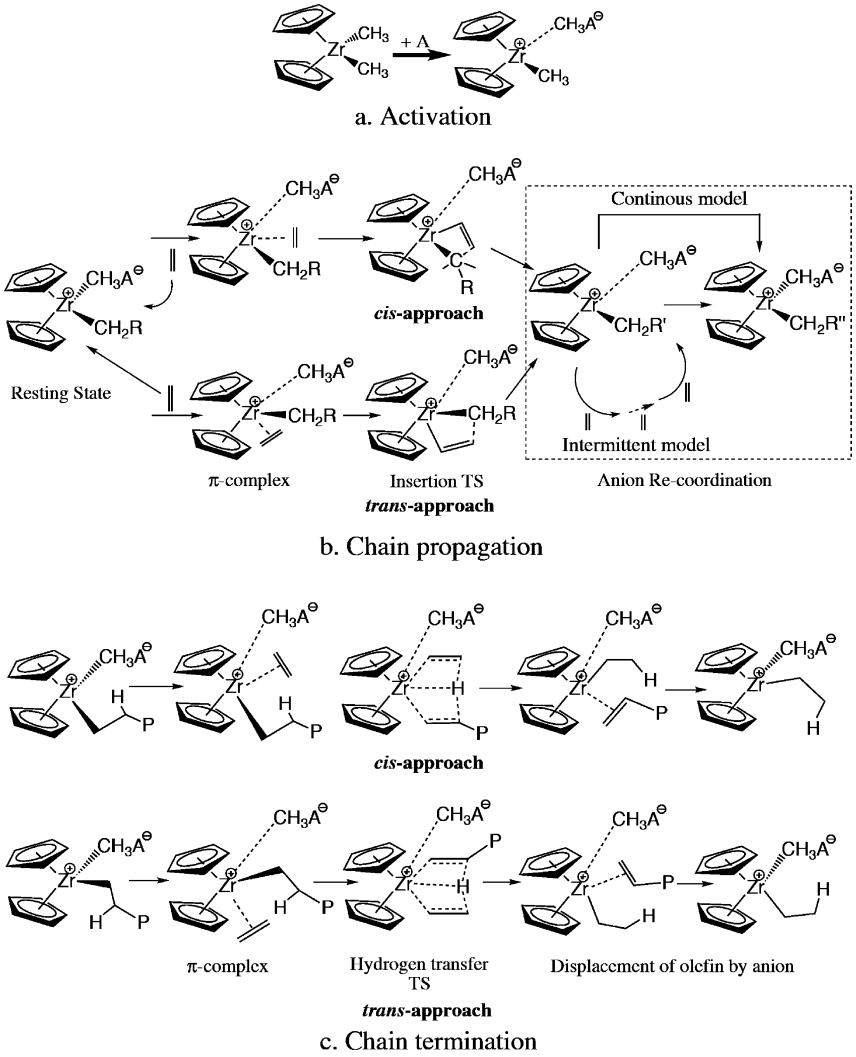

different levels of static *ab initio* quantum mechanics (QM) or combined quantum mechanics and molecular mechanics (QM/MM) calculations. As a result of these efforts, a generally accepted mechanism for polymer chain propagation and termination has been established, as depicted in Scheme 1b,c, respectively. The catalyst activation by a Lewis acid (Scheme 1a) leads to the contact ion pair $[Cp_2ZrMe]^+[MeA]^-$ kept together in a μ-CH_3 fashion (referred to as a bridged ion pair later). Uptake of the olefin by the ion pair takes place in an attack by the monomer either *cis* or *trans* to the counteranion. For the chain propagation (Scheme 1b), the monomer displaces the counteranion to form a weak π-complex in an associative way (S_N2 type), in which there in the end is no bonding interaction between the ion pair (referred to as the nonbonded ion pair hereafter), followed by ethylene insertion into the Zr−C bond to achieve the enchainment. The chain termination occurs by the transfer of a β-hydrogen on the polymer chain to a π-coordinated monomer (Scheme 1c).

Some detailed aspects of the role played by the counteranion are still controversial, including the degree of counteranion mobility.[1a,13,14] The accepted mechanism is that the counteranion dissociates to some degree during the first ethylene insertion process. However, it has been debated whether the ion pair manage to recombine before each subsequent insertion. This will clearly depend on whether the recombination is fast or slow relative to the rate of propagation. A slower recombination rate will lead to an intermittent mechanism of propagation, in which the displacement of the counteranion by the ethylene monomer is an infrequent reinitiation event that is followed by a burst of propagations before the anion recoordination occurs (see the part in the dashed rectangle, Scheme 1b). A faster rate of ion-pair reassociation suggests, on the other hand, a continuous propagation model, in which the ion-pair recombination occurs after each insertion step. Experimentally, Schaper et al.[13] have suggested the intermittent mechanism, on the basis of the fact that the displacement rate of $[MeB(C_6F_5)_3]^-$ by Lewis bases is rather slow. However, recently Landis et al.[14] have argued in favor of the continuous mechanism on the basis of direct in

(9) Fusco, R.; Longo, L.; Proto, A.; Masi, F.; Garbassi, F. *Macromol. Rapid. Commun.* **1998**, *19*, 257.

(10) Nifant'ev, I. E.; Ustyyuk, L. Y.; Laikov, D. N. *Organometallics* **2001**, *20*, 5375.

(11) (a) Chan, M. S. W.; Vanka, K.; Pye, C. C.; Ziegler, T. *Organometallics* **2000**, *19*, 5182. (b) Xu, Z.; Vanka, K.; Ziegler, T. *Organometallics* **2004**, *23*, 104. (c) Zurek, E.; Ziegler, T. *Faraday Discuss.* **2003**, *93*. (d) Vanka, K.; Xu, Z.; Ziegler, T. *Isr. J. Chem.* **2003**, 42. (e) Vanka, K.; Xu, Z.; Ziegler, T. *Can. J. Chem.* **2003**, *81*, 1413.

(12) (a) Bernardi, E.; Bottoni, Z.; Miscione, G. P. *Organometallics* **1998**, *17*, 16. (b) Schaper, F.; Geyer, A.; Brintzinger, H. H. *Organometallics* **2002**, *21*, 473.

(13) (a) Schaper, F.; Geyer, A.; Brintzinger, H. H. *Organometallics* **2002**, *21*, 473. (b) Fink, G.; Fenzl, W.; Mynott, R. Z. *Naturforsch., B* **1985**, *406*, 158.

(14) Landis, C. R.; Rosaaen, K. A.; Sillars, D. R. *J. Am. Chem. Soc.* **2003**, *125*, 1710.

situ observations of the whole catalytic process. So far, this issue has not been addressed by theoretical methods. The main problem is that the traditional static QM or QM/MM methods are unable to address this question. However, methods based on molecular dynamics (MD) might be of use in this case. We shall in the current study present calculations on the ion-pair recombination based on the MD method. Further, MD methods are well suited to evaluate free energy profiles for a catalytic process, a task that can be expensive and inaccurate with static methods where use is made of the harmonic approximation. To the best of our knowledge, most dynamic studies on polymerization have dealt with the naked cation.[15,16] Only one investigation[17] describes in a short dynamic simulation the insertion of one molecule of ethylene into the Zr−Et bond of the $[Cp_2ZrEt]^+[MeB(C_6F_5)_3]^-$ ion pair.

In this account, we employ the Car−Parrinello ab initio molecular dynamics (CP-AIMD) method[18] in an investigation of the whole catalytic polymerization cycle, including chain propagation and chain termination with the counteranion included, as shown in Scheme 1b,c. One of the objectives has been to analyze the role played in the catalytic process by the counteranion. We shall to this end provide an accurate free energy profile based on well-equilibrated simulations. We hope that MD can provide a more realistic energy profile in which many of the statistically unimportant finer details on the potential energy profile are "washed out" by entropy. Solvation effects will be taken into account by the use of a continuum model. A comparison will be made to the very recent static QM/MM study on the same system by Vanka et al.[19] and to the study given in ref 10.

2. Computational Details

All calculations were carried out with the Car−Parrinello projector augmented wave (CP-PAW) code developed by Blöchl[20,21] and extended by Woo et al.[22] to combine quantum mechanics and molecular mechanics (CP-PAW-QM/MM). The partition scheme developed by Morokuma and Maseras[23] and augmented by Woo et al.[24] was used to couple the QM and MM regions. Except for the anion $CH_3-B(C_6F_5)_3^-$, all parts of the system were described by QM. The anion was represented by a validated QM/MM model[11e] where the QM part consisted of $CH_3-BCl_3^-$, whereas the three C_6F_5 groups were described by MM. A ratio, α, of 0.884 was adopted for the B−C(aryl) link bonds, to reproduce the average experimental bond distances in related compounds.[24]

In the calculation of the QM part, the DFT functional used was that formed by the combination of the Perdew−Wang parametrization of the electron gas[25] in conjunction with the exchange gradient correction presented by Becke[26] and the correlation correction of Perdew.[27,28] Periodic boundary conditions were used, with a unit cell described by the lattice vectors ([0, 18.0, 18.0], [18.0, 0, 18.0], [18.0, 18.0, 0] (Å)). These unit cells were sufficiently large to ensure negligible overlap of the wave functions with the periodic images. In all of the calculations the molecules have been electrostatically decoupled from their periodic images as described in ref 29. The energy cutoff used to define the basis set was 30 Ry (15 au) in all cases. The SHAKE algorithm[30] was used to impose constraints.

In the calculation of the MM region, an augmented AMBER95[31] molecular mechanics force field was utilized to describe the molecular mechanics potential. Also, this region was oversampled by a 20:1 ratio[32] over the QM region to enhance the sampling of the large and "floppy" aryl rings.[33,34]

The mass of hydrogen atoms was taken to be that of deuterium, and normal masses were taken for all other elements except the chlorine link atoms. The mass of the chlorine link atoms was taken to be the same as that of carbon.

The free energy (ΔA) calculated here is the Helmholtz free energy, corresponding to an NVT ensemble. Within a canonical (NVT) ensemble, the change in the Helmholtz free energy ΔA between two states, a and b, is given according to the thermodynamic integration method as

$$\Delta A_{a\to b} = \int_a^b \left\langle \frac{\partial E(X,s)}{\partial s} \right\rangle_s \mathrm{d}s = -\int_a^b \langle F_s \rangle \, \mathrm{d}s \qquad (1)$$

Here s is a running parameter for the progress along the reaction coordinate, E represents the potential energy of the system as a function of the $3N$ spatial coordinates, X, with the constraint s. Further, F_s is the force acting on the chosen constraint. The brackets indicate an ensemble average of the system at the constraint value s. The integral of eq 1 is typically evaluated through a finite difference numerical integration scheme referred to as pointwise thermodynamic integration (PTI).[35] In the PTI scheme, a small number of points along the reaction coordinate are chosen, and the system is allowed to dynamically evolve and sample phase space at each point for a long time with no data collected between each point. The average force at each point is then used as the ensemble average of the force in eq 1. Enough points (10−40, depending on the length of the reaction coordinate and the shape of the free energy profile) along the reaction coordinate were taken to ensure that the numerical integration performed later was sufficiently accurate (numerical error <0.5 kcal/mol). At each of these values of the reaction coordinate a 2.3 ps trajectory was calculated, but only the last 1.9 ps[36] of the simulation was used to obtain the ensemble average of the constraint force $\langle F_s \rangle$ at the value s for the reaction coordinate. These average forces at each value of the reaction

(15) Margl, P.; Lohrenz, J. C. W.; Ziegler, T.; Blöchl, P. E. *J. Am. Chem. Soc.* **1996**, *118*, 4434.
(16) Meier, R. J.; van Dormaele, G. H. J.; Iarlori, S.; Buda, F. *J. Am. Chem. Soc.* **1994**, *116*, 7274.
(17) Chan, M. S. W.; Ziegler, T. *Organometallics* **2000**, *19*, 5182.
(18) Car, R.; Parrinello, M. *Phys. Rev. Lett.* **1985**, *55*, 2471.
(19) Ziegler, T.; Vanka, K.; Xu, Z. *C. R. Chim.* **2005**, 8.
(20) Blöchl, P. E. *Phys. Rev. B* **1994**, *50*, 17953.
(21) Blöchl, P. E. *J. Phys. Chem.* **1995**, *99*, 7422.
(22) Woo, T. K.; Blöchl, P. E.; Ziegler, T. *J. Phys. Chem. A* **2000**, *104*, 121.
(23) Maseras, F.; Morokuma, K. *J. Comput. Chem.* **1995**, *16*, 1170.
(24) Woo, T. K.; Cavallo, L.; Ziegler, T. *Theor. Chem. Acc.* **1998**, *100*, 307.
(25) Perdew, J. P.; Wang, Y. *Phys. Rev. B* **1992**, *45*, 13244.
(26) Becke, A. *Phys. Rev. A* **1988**, *38*, 3098.
(27) Perdew, J. P. *Phys. Rev. B* **1986**, *34*, 7406.
(28) Perdew, J. P. *Phys. Rev. B* **1986**, *33*, 8822.
(29) Blöchl, P. E. *J. Chem. Phys.* **1995**, *103*, 7422.
(30) Ryckaert, J. P.; Cicotti, G.; Berensden, H. J. *J. Comput. Phys.* **1977**, *23*, 327.
(31) Clark, M.; Cramer, R. D., III; van Opdenbosch, N. *J. Comput. Chem.* **1989**, *10*, 982.
(32) The oversampling was achieved as follows: providing the time step for the QM region is Δt, and then the time step is $\Delta t/20$ for the MM region. The QM and MM regions were propagated asynchronously. At the moment of $T = t_0$, for example, the MM region was first propagated to $t_0 + \Delta t/2$, which is 10 time steps. Then, the QM region was propagated to $t_0 + \Delta t$; following that, the MM region was propagated from $t_0 + \Delta t/2$ to $t_0 + \Delta t$ (passing the second set of 10 time steps ($\Delta t/2$)). The rationality and advantages of this scheme have been validated by Woo.[33]
(33) Woo, T. K.; Margl, P.; Blchl, P.; Ziegler, T. *J. Phys. Chem. A* **2002**, *106*, 1173.
(34) Woo, T. K.; Margl, P. M.; Deng, L.; Cavallo, L.; Ziegler, T. *Catal. Today* **1999**, *50*, 479.
(35) Straatsma, T. P.; McCammon, J. A. *J. Chem. Phys.* **1991**, *95*, 1175.
(36) One of the reviewers was concerned about the convergence of the force. We made a test for the cis pathway of the first insertion step. The force at each point was calculated by averaging over the last 2.7 ps. Very little difference (less than 0.0003 hartree/bohr) was obtained between the forces obtained by averaging the last 2.7 and 1.9 ps, which shows that the mean force converges very well. Further, the difference in the free energy changes is less than 0.5 kcal/mol. No obvious change can be found for the free energy profiles.

Scheme 2

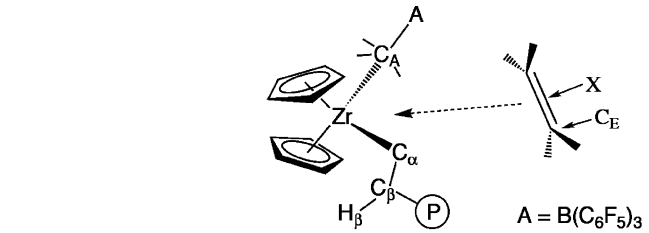

Nomenclature

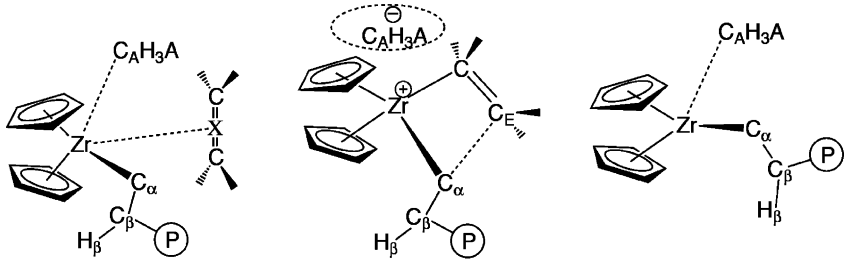

Reaction coordinates for chain propagation

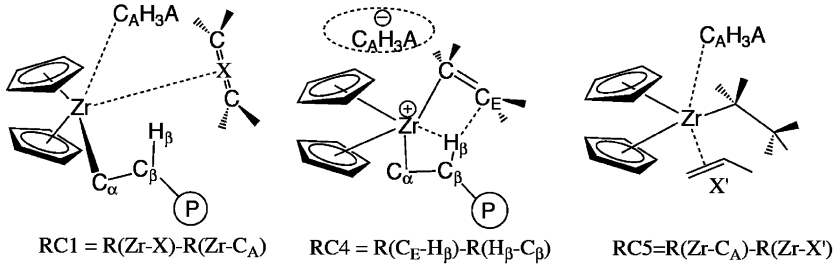

Reaction coordinates of chain termination

coordinate were integrated by Simpson's method to obtain the free energy change ΔA according to eq 1.

The stochastic thermostat of Andersen,[37] which was considered as a more suitable thermostat in the case of free energy integration,[38a] was used in the QM part. The thermostat settings were monitored and adjusted if necessary during the equilibration stage, with the main criteria for adequate thermostating being that the mean temperature was within a range of 300 ± 15 K and the temperature drift lower than 1.5 K/ps. In combination with the Andersen thermostat, a constant friction was applied to the wave function with a value of 0.005. The classical Nosé−Hoover thermostat,[39] a dynamical friction-based thermostat, was performed in the MM part.

To determine the finite temperature or entropy effect, the potential energy profile (PEP) was calculated by the same program. A linear constraint along the reaction coordinate was used to generate the potential energy curve. In some regions, such as near the intermediates, in which the ion pair was separated by 3−5 Å, the optimization had to be repeated from different starting geometries in order to obtain the geometry with the lowest energy, due to the existence of many local minima as a result of the many possible relative orientations of the two ions in the ion pair.

The conductor-like screening model (COSMO)[40] was used to estimate the solvation energies. The geometries used at each point along the reaction coordinates were the averaged ones from the dynamic simulations at each PTI step. Only the electrostatic contribution to the solvation energy was calculated. Cyclohexane, with a dielectric constant of 2.023, was used as the solvent. The radii used for the atoms (in Å) were as follows: 2.0 (C), 1.16 (H), 1.15 (B), 1.2 (F), and 2.4 (Zr). This part was calculated by the ADF program.[41]

All simulations were carried out with the translation of the center of mass and rotation of the total system removed. A correction to the entropy due to the neglect of the total translational and rotational motion was conducted by following the scheme outlined in ref 38. It should be mentioned that the zero-point energy (ZPE) correction is not included in our simulations.

3. Results and Discussion

3.1. Nomenclature and Reaction Coordinates. Before we present results from the dynamic simulations, we shall provide a brief introduction to the nomenclature and the reaction coordinates used here in order to facilitate the discussion given later in this paper.

Scheme 2 illustrates the notations for some important atoms. C_A denotes the carbon atom of the methyl group which was abstracted by the Lewis acid A (=$B(C_6F_5)_3$) in the catalyst

(37) Andersen, H. C. *J. Chem. Phys*. **1980**, *72*, 2384.

(38) (a) Kelly, E.; Seth, M.; Ziegler, T. *J. Phys. Chem. A* **2004**, *108*, 2167. (b) Yang, S.-Y.; Fleurat-Lessard, P.; Hristov, I.; Ziegler, T. *J. Phys. Chem. A* **2004**, *108*, 9461.

(39) (a) Nosé, S. *Mol. Phys*. **1986**, *57*, 187. (b) Hoover, W. G. *Phys. Rev. A: At. Mol. Opt, Phys.* **1985**, *31*, 1695.

(40) (a) Klamt, A.; Schuurmann, G. *J. Chem. Soc., Perkin Trans. 2* **1993**, 799. (b) Pye, C. C.; Ziegler, T. *Theor. Chem. Acc*. **1999**, *101*, 396.

(41) (a) Baerends, E. J.; Ellis, D. E.; Ros, P. *Chem. Phys*. **1973**, *2*, 41. (b) Baerends, E. J.; Ros, P. *Chem. Phys*. **1973**, *2*, 52. (c) te Velde, G.; Baerends, E. J. *J. Comput. Phys*. **1992**, *99*, 84. (d) Fonseca, C. G.; Visser, O.; Snijders, J. G.; te Velde, G.; Baerends, E. J. In *Methods and Techniques in Computational Chemistry, METECC-95*; Clementi, E., Corongiu, G., Eds.; STEF: Cagliari, Italy, 1995; p 305.

activation step (Scheme 1a). C_α and C_β are the α- and β-carbon atoms in the polymer chain, respectively; H_β is a β-hydrogen on the polymer chain. C_E is one of the ethylene carbons. X represents the mass center of the C═C bond in ethylene.

Due to the complexity of the reaction, it is difficult to describe the whole process with one reaction coordinate, unless use is made of the intrinsic reaction coordinate (IRC),[42] which is computationally too demanding at the present time. Therefore, different reaction coordinates were used at different parts of the catalytic cycle (Scheme 2). For ethylene uptake by the metal center and the counteranion dissociation, the distance difference between R(Zr−X) and R(Zr−C_A) was chosen as the reaction coordinate (RC1). We avoided just using the simple distance R(Zr−X) as the reaction coordinate, because it cannot describe the S_N2-type mechanism that has been commonly accepted for the displacement of the counteranion by ethylene. The distance R(C_E−C_α) was used as the reaction coordinate for the ethylene insertion (RC2). For the possible counteranion recoordination to the metal center after the ethylene insertion, the distance R(Zr−C_A) was chosen as the reaction coordinate (RC3). The H_β transfer in the termination step was described by a reaction coordinate taken as the distance difference between R(C_E−H_β) and R(H_β−C_β) (RC4). Finally, for the displacement by the anion of the olefin produced by H_β transfer to the olefin monomer, we used the distance difference RC5 = R(Zr−C_A) − R(Zr−X′) (X′ denotes the mass center of the C═C bond in the olefin) as the reaction coordinate.

3.2. Energy Profile for Heterolytic Dissociation of the Bridged Ion Pair. In the course of the catalytic cycle the initially bridged ion pair [$Cp_2ZrR(\mu$−Me)$B(C_6F_5)_3$] formed in the catalyst activation step (Scheme 1a) will dissociate to the nonbonded ion pair $[Cp_2ZrMe]^+[MeA]^-$, which potentially can recombine after the ethylene insertion. It might thus be useful as a prerequisite for studies of the chain propagation and termination to explore the FEP and PEP for the ion-pair dissociation. Lanza et al.[43] have calculated the potential energy profile for the heterolytic $[H_2Si(C_5H_4)(^tBuN)Ti(CH_3)]^+[CH_3B(C_6H_5)_3]^-$ cleavage. They found that the potential energy increases linearly along the Ti^+- - -$[CH_3B(C_6H_5)_3]^-$ distance, while the bridging bond is broken. After that, the energy resembles the isotropic Coulombic attraction between the $[H_2Si(C_5H_4)(^tBuN)Ti(CH_3)]^+$ and $[CH_3B(C_6H_5)_3]^-$ ions. We present here both the FEP and PEP for the dissociation of [$Cp_2ZrMe(\mu$-Me)$B(C_6F_5)_3$] in order to assess the influence of entropy.

We shall focus on the range R(Zr−C_A) = 2.4−5.0 Å, where the Zr−(μ-CH_3)−$B(C_6F_5)_3$ bond gradually is broken and replaced by the Coulombic interaction between $[Cp_2ZrCH_3]^+$ and $[CH_3B(C_6F_5)_3]^-$. It can be seen that both the FEP and PEP are continuously increasing on going from their minima to 5.0 Å without any barrier. The PEP reveals, as in the study by Lanza et al.,[43] a linear increase followed at ∼4.0 Å by a Coulombic asymptote after the bridging Zr−(μ-CH_3)$B(C_6F_5)_3$ bond has broken. The FEP exhibits a shift in the equilibrium distance for R(Zr−C_A) to 2.7 Å, compared to 2.52 Å for PEP. The shift is due to thermal motion. We note further that the FEP drops below the PEP during the dissociation progress, due to an increase in the entropy. At R = 5 Å, FEP has dropped ca. 10 kcal/mol below PEP. The structures A1−A3 in Figure 1 are "snapshots" along the dissociation path where the bridged bond gradually breaks. From the snapshots, one can notice that the nonbridged ion pair prefers to adopt an orientation where the methyl group in the counteranion $[CH_3-B(C_6F_5)_3]^-$ is oriented along the alkyl chain in order to minimize steric interaction.

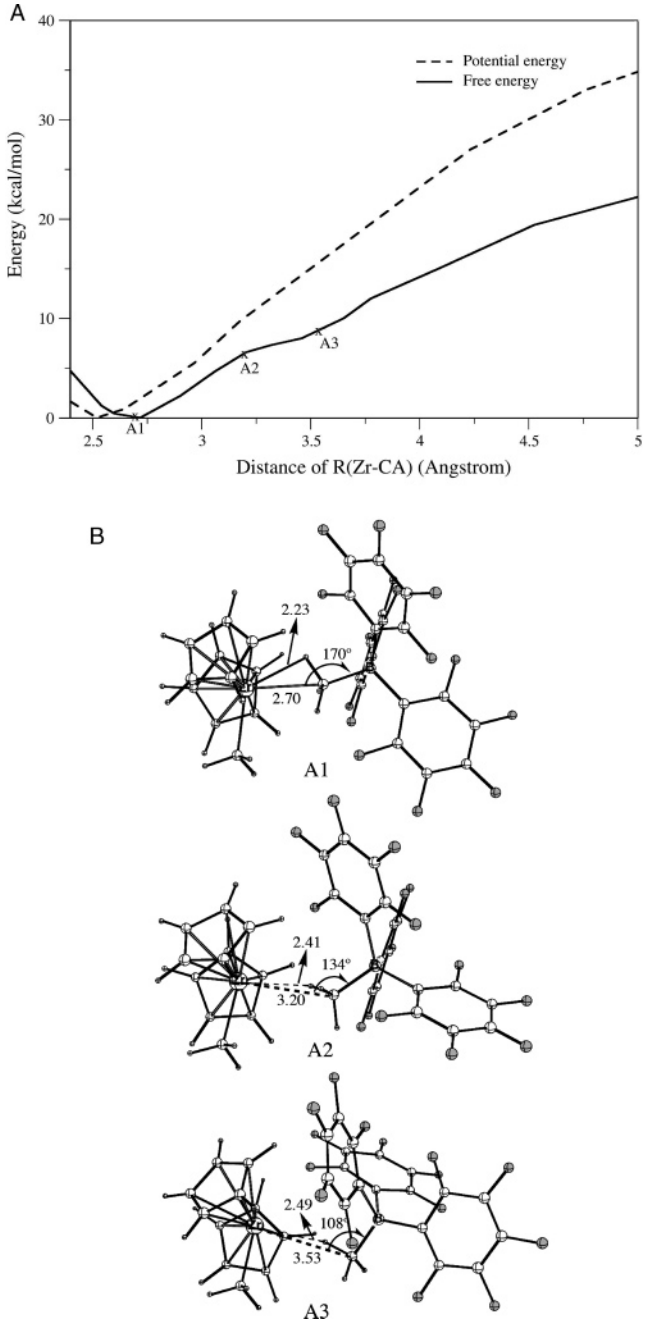

Figure 1. Potential energy profile (0 K) and free energy profile (300 K) for the ion-pair $[Cp_2ZrCH_3]^+[CH_3B(C_6F_5)_3]^-$ dissociation. A1, A2, and A3 are three snapshots from the dynamic simulation. Distances are given in Å.

3.3. Chain Propagation. The chain propagation involves pathways in which ethylene approaches the metal center *cis* or *trans* to the counteranion, respectively. The whole propagation pathway was split into three phases for both the *cis* and *trans* approach: ethylene uptake, insertion, and counteranion recombination. The three phases are described by the reaction coordinates RC1, RC2, and RC3, respectively. RC1 = R(Zr−X) − R(Zr−C_A) was started from the value of 2.65 Å, where R(Zr−X) has a distance of 5.0−5.5 Å. At that Zr−X distance, the interaction between Zr and ethylene is minimal. The first phase ends with the formation of the π-complex, where the force dE/dRC1 is close to zero (dE/dRC1 < 5×10^{-4} hartree/bohr). The starting value of RC2 of the insertion was chosen as the

(42) Fukui, K. *Acc. Chem. Res.* **1981**, *14*, 363.
(43) Lanza, G.; Fragalà, I.; Marks, T. J. *Organometallics* **2002**, *21*, 5594.

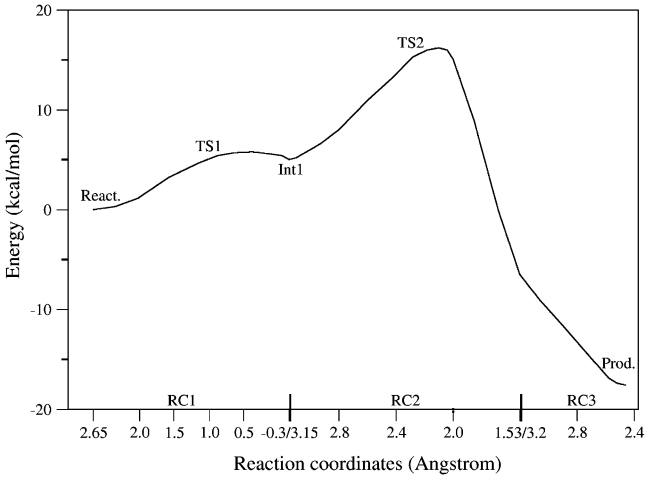

Figure 2. Potential energy profiles for the ethylene uptake, insertion, and ion-pair recombination in the cis path of the first insertion step.

distance $R(C_E-C_\alpha)$ from the π-complex just formed. The final value of RC2 is 1.53 Å, which corresponds to a regular C−C single-bond length. In the actual simulations, it was found that the counteranion has a strong preference for recombining with the metal center when RC2 is close to 1.53 Å, due to the fact that the recombination is barrierless (see section 3.2). To separate insertion from recombination, we added another constraint on the distance $R(Zr-C_A)$ when RC2 is around 1.53 Å. The constraint value was chosen as 3.2 Å for 0 K, since 3.2 Å represents the breaking point for the bridged bond as discussed before, and 3.4 Å for 300 K, which is an estimated average distance of $Zr-C_A$ after ethylene insertion, as will be seen later. This constraint has only a minor influence (less than 1 kcal/mol) on the final part of PEP and FEP. The recombination phase represented by RC3 starts at 3.2 (0 K)/3.4 Å (300 K) and ends at 2.52 (0 K)/2.70 Å (300 K) with formation of the product.

3.3.1. The First Insertion Step. We study the polymer chain propagation from the very beginning, where the ion pair [Cp_2-ZrMe(μ-Me)B(C_6F_5)$_3$] is the resting state. Both the *cis* and the *trans* approaches will be considered.

a. *cis* Approach. Potential Energy Profile. The three phases involved in the *cis* approach are described by the three reaction coordinates RC1, RC2, and RC3, respectively. RC1, which is for the ethylene uptake, varies from 2.65 Å to the π-complex formation at −0.3 Å, RC2 , which is for the ethylene insertion, varies from 3.15 Å at the π-complex to 1.53 Å, and RC3, which is for the recombination of the nonbridged ion pair, ranges from 3.2 to 2.52 Å. The calculated potential energy curves of the three phases are displayed in one graph in Figure 2. Table 1 gives the calculated energies for the reactant, transition states, π-complex, and product.

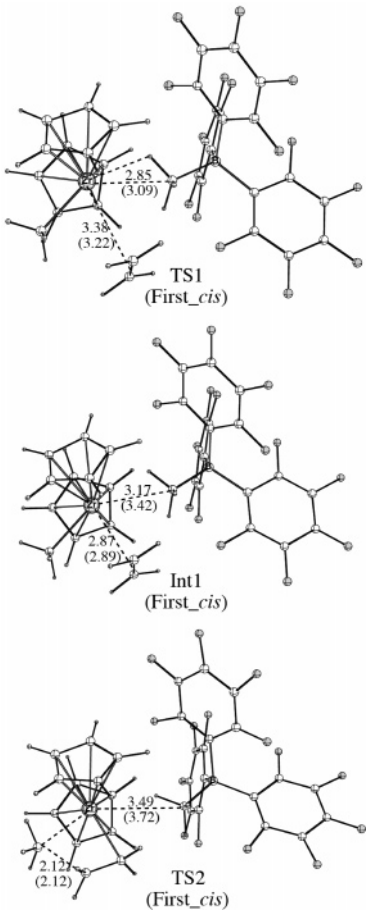

Figure 3. Calculated structures and selected bond distances for the transition state of ethylene uptake (TS1), ethylene π-complex (Int1), and insertion transition state (TS2) in the cis path of the first insertion step at 0 K (values in parentheses are the averaged bond distances at 300 K). Distances are given in Å.

The PEP exhibits two peaks corresponding to the transition states for ethylene uptake (TS1) and insertion (TS2). In the middle of the two peaks there is a very shallow well representing the ethylene π-complex (Int1). In the transition state of ethylene uptake, the distances of Zr−X and $Zr-C_A$ are 3.38 and 2.85 Å, respectively (see Figure 3), which indicates that the ethylene π-complex is under formation and the ion pair is starting to break up. The uptake barrier is 6.0 kcal/mol, comparable with 4.5 kcal/mol obtained by ADF.[19] The resulting π-complex with

Table 1. Calculated Relative Energies (kcal/mol) for the Reactant, Ethylene Uptake Transition State (TS1), Ethylene π-Complex (Int1), Insertion Transition State (TS2), and Product in the First and Second Ethylene Insertion Steps

		reactant	TS1	Int1	TS2	product
		First Step				
cis	potential energy in gas phase (0 K)	0.0	6.0	5.3	16.2	−17.5
	free energy in gas phase (300 K)	0.0	15.4	12.6	23.3	−6.3
	free energy with solvation (300 K)	0.0	14.7	10.7	18.2	−5.6
trans	potential energy in gas phase (0 K)	0.0	15.9	15.0	15.3	−17.4
	free energy in gas phase (300 K)	0.0	20.2	18.8	23.6	−7.0
	free energy with solvation (300 K)	0.0	16.2	13.8	18.5	−6.2
		Second Step				
cis	potential energy in gas phase (0 K)	0.0	9.6	3.9	12.5	−18.5
	free energy in gas phase (300 K)	0.0	17.8	12.0	24.1	−9.0
	free energy with solvation (300 K)	0.0	16.3	7.5	17.2	−9.3
trans	potential energy in gas phase (0 K)	0.0	16.3	14.2	14.5	−18.3
	free energy in gas phase (300 K)	0.0	20.5	18.7	24.8	−7.8
	free energy with solvation (300 K)	0.0	17.7	14.1	19.6	−8.4

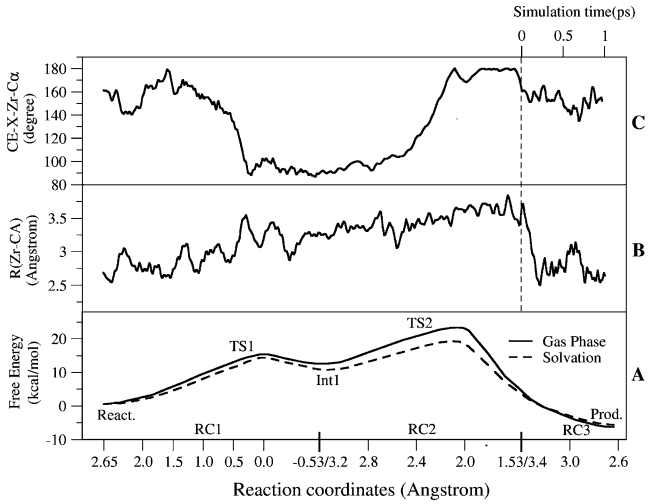

Figure 4. (A) Free energy profiles (300 K) for the ethylene uptake, insertion, and ion-pair recombination in the cis path of the first insertion step. (B) $Zr-C_A$ distance changes along the reaction coordinates of RC1 and RC2. The right part of the dashed line gives the $Zr-C_A$ distance changes in the dynamic simulation without any constraint. (C) Dihedral angle $C_E-X-Zr-C_\alpha$ variations along the reaction coordinates of RC1 and RC2. The right part of the dashed line gives the dihedral angle $C_E-X-Zr-C_\alpha$ variations in the dynamic simulation without any constraint.

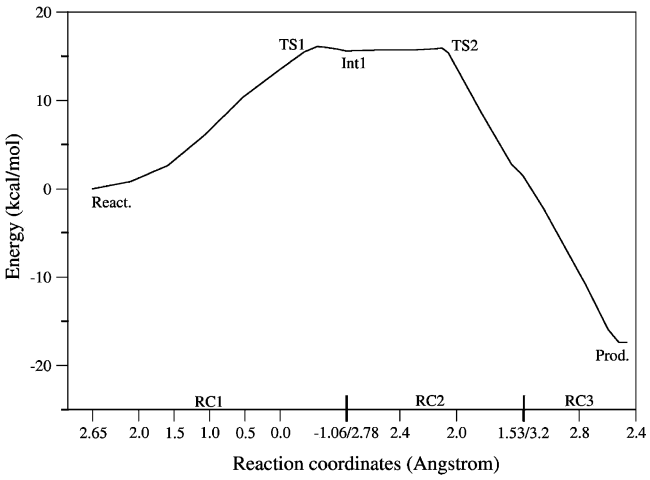

Figure 5. Potential energy profiles for the ethylene uptake, insertion, and ion-pair recombination in the trans path of the first insertion step.

an energy of 5.3 kcal/mol has a $Zr-X$ distance of 2.87 Å and a $Zr-C_A$ length of 3.17 Å. This indicates that the ion-pair bridge has almost broken in the π-complex. At the TS2, the $Zr-C_A$ distance is 3.49 Å, which signals that the ion-pair bridge is fully broken. TS2 affords the highest energy point (16.2 kcal/mol) on the PEP. The insertion barrier is due to the ion-pair separation as well as the breaking of the $Zr-C_\alpha$ bond. The insertion barrier calculated here is very close to the corresponding value obtained by a static DFT calculation (16.7 kcal/mol).[19]

300 K Free Energy Profile. The calculated FEPs for the *cis*-approach along the same coordinates RC1, RC2 and RC3 as those at 0 K, are displayed in Figure 4A, although their ranges have been changed a bit. The relative free energy changes are given in Table 1.

Comparing the FEP and PEP, one observes two distinct differences. One is the higher barriers on the FEP for both the ethylene uptake and insertion. Another difference is that the π-complex resides in a somewhat deeper well on the FEP. For the transition state of ethylene uptake, the average distances of $Zr-X$ and $Zr-C_A$ are 3.22 and 3.09 Å, respectively (see Figure 3), which are longer compared to the corresponding value on the PEP. The distance changes from 0 to 300 K are due to the thermal motion. The uptake barrier is 15.4 kcal/mol on the FEP, which is 9.4 kcal/mol higher than that on the PEP. The difference can be attributed to the entropy contribution $-T\Delta S$ to ΔA. This entropy contribution obtained here is very close to the value of 11.1 kcal/mol found in a static calculation with use of the harmonic approximation.[10] The ethylene π-complex has the ethylene perpendicular to the $CH_3-Zr-CH_3A^-$ plane, according to the trajectory obtained in the slow growth simulation. The distances of $Zr-X$ and $Zr-C_A$ in the π-complex are 2.89 and 3.42 Å, respectively, which indicates that the ion-pair bridge is fully broken. The deeper well for the π-complex on the FEP compared to the PEP is due to the extra entropic stabilization due to the ion-pair separation. In the insertion transition state (TS2), the ethylene rotates to the "in-plane" orientation in order to facilitate the insertion. As a result, the ion pair is further separated to 3.72 Å in order to reduce the accumulated steric strain in the equatorial plane. The TS2 has the highest energy on the FEP (23.3 kcal/mol). The barrier is due to the large separation of the ion pair and the breakage of the $Zr-C_\alpha$ bond.

To monitor the motion of the counteranion and the incoming monomer, we have performed slow growth simulations for ethylene uptake and insertion, in which RC1 was varied slowly from 2.65 to −0.53 Å and RC2 from 3.2 to 1.53 Å, whereas the remaining degrees of freedom were allowed to propagate freely. We finally carried out an unconstrained simulation of the ion-pair recombination along RC3 to monitor the rate of counteranion reassociation to the metal center. The distance change of $R(Zr-C_A)$ and the torsion angle variation of $C_E-X-Zr-C_\alpha$ in the simulation are displayed in parts B and C of Figure 4, respectively. Clearly, in the initial stage, when ethylene approaches the zirconium center, the anion starts to move away from the zirconium. When the π-complex is formed, the $Zr-C_A$ distance has an average value of 3.4 Å, and the dihedral angle of $C_E-X-Zr-C_\alpha$ is ca. 90°, which means that the ethylene coordinates to the zirconium center in a perpendicular (to the $CH_3-Zr-CH_3A$ plane) fashion. Around the insertion transition state, the counteranion goes slightly further from the zirconium center (average 3.7 Å). After that, the anion rapidly reassociates to the zirconium again to form a bridged ion pair in a period that is less than 0.5 ps.

Solvation-Corrected FEP. The FEP including solvation effects is displayed in Figure 4A (dashed line). The solvation slightly reduces the energy of TS1, but significantly stabilize the transition state of insertion by ca. 5 kcal/mol (see Table 1). This is reasonable because in TS2 the ion-pair has the maximum $Zr-C_A$ distance, Figure 4B, and hence the largest charge separation.

b. *trans* Approach. Potential Energy Profile. For the *trans* pathway, the monomer approaches the metal center from a position that is *trans* to the counteranion [CH_3A^-]. The reaction coordinates used here are RC1 for the ethylene uptake, which varies from 2.65 to −1.06 Å, RC2 for the ethylene insertion, which varies from 2.78 to 1.53 Å, and RC3 for the counteranion recombination, which varies from 3.2 to 2.52 Å. Figure 5 displays the calculated potential energy profiles along the reaction coordinates. We note a very flat region between TS1 and TS2 and a very shallow well (ca. 0.9 kcal/mol) corresponding to the π-complex. The energies of TS1 and TS2 are 15.9 and 15.3 kcal/mol, respectively (Table 1). The previous static

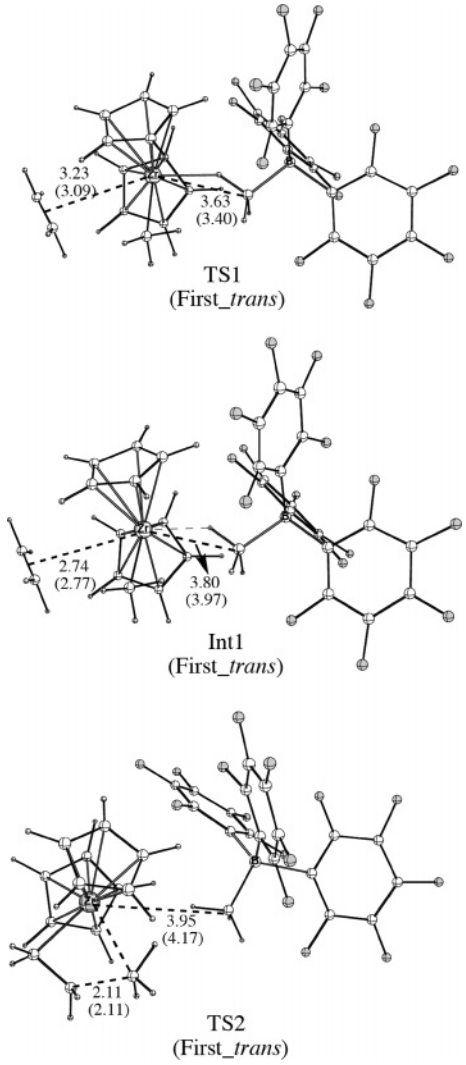

Figure 6. Calculated structures and selected bond distances for the transition state of ethylene uptake (TS1), ethylene π-complex (Int1), and insertion transition state (TS2) in the trans path of the first insertion step at 0 K (values in parentheses are the averaged bond distances at 300 K). Distances are given in Å.

DFT calculation[19] failed to locate the TS1, which is not surprising, considering the shallow shape of the PEP.

The geometry parameters for TS1, Int1, and TS2 are shown in Figure 6. The monomer ethylene approaches the metal center in an "in-plane" fashion. This leads to the notion that the ion pair is fully separated as early as at the stage of the uptake transition state (the $Zr-C_A$ distance is 3.63 Å; Figure 6) in order to provide coordination space for ethylene. In the π-complex, the ion pair is further separated to 3.80 Å. This, however, does not increase the total energy of the π-complex, due to the stronger interaction between zirconium and ethylene in Int1 compared to TS1. In the insertion transition state, the $Zr-C_A$ distance is further elongated to 3.95 Å. Nevertheless, the total energy does not increase considerably from Int1 to TS2.

Free Energy Profile at 300 K. We adopted the same reaction coordinates, RC1, RC2, and RC3, as those used at 0 K, with a small change in their ranges due to the temperature effect. The free energy profiles are displayed in Figure 7. The free energy barrier for TS1 increases by 4.3 kcal/mol over the potential energy barriers, which is due to the entropy contribution $-T\Delta S$. The ethylene uptake by the catalyst will have a negative entropy contribution. However, the concurrent dissociation of the ion pair gives a positive entropy contribution. Cancellations in the

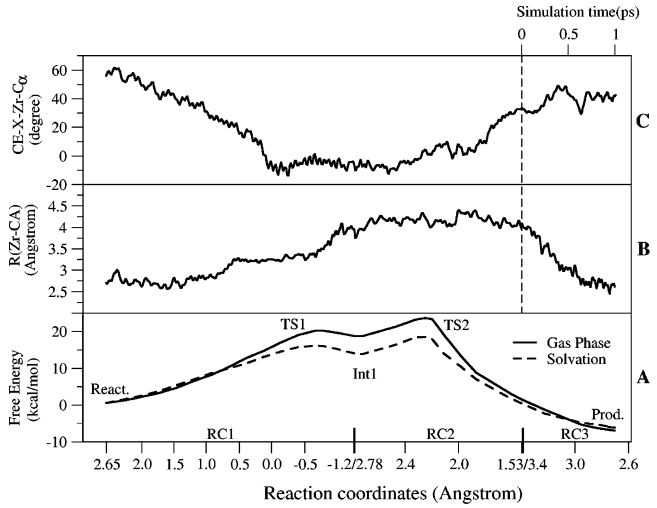

Figure 7. (A) Free energy profiles (300 K) for the ethylene uptake, insertion, and ion-pair recombination in the trans path of the first insertion step. (B) $Zr-C_A$ distance changes along the reaction coordinates of RC1 and RC2. The right part of the dashed line is the $Zr-C_A$ distance changes in the dynamic simulation without any constraint. (C) Dihedral angle $C_E-X-Zr-C_\alpha$ variations along the reaction coordinates of RC1 and RC2. The right part of the dashed line gives the dihedral angle $C_E-X-Zr-C_\alpha$ variations in the dynamic simulation without any constraint.

sum of the two entropy terms leads to a modest contribution from $-T\Delta S$. In the π-complex, the counteranion moves slightly further from the zirconium center (the $Zr-C_A$ distance is 3.97 Å; Figure 6). The stabilizing entropy contribution due to the additional separation of the ion pair, as well as the π-interaction between zirconium and ethylene, is responsible for the deeper well of the π-complex on the FEP compared to that on the PEP. In the insertion transition state, the $Zr-C_A$ distance is further increased to 4.17 Å. The free energy barrier is 23.6 kcal/mol.

To monitor the detailed molecular motion, three separate simulations, including two slow-growth trajectories for RC1 and RC2 and a simulation without any constraint for RC3, were performed. The distance change of $R(Zr-C_A)$ and the torsion angle variation of $C_E-X-Zr-C_\alpha$ in the simulations are displayed in parts B and C of Figure 7, respectively. As the monomer ethylene approaches the zirconium center, the anion is increasingly displaced. In the ethylene π-complex, the $Zr-C_A$ distance has an average distance of ca. 3.4 Å, and the dihedral angle of $C_E-X-Zr-C_\alpha$ is close to 0, which means that ethylene approaches the catalyst in an in-plane fashion (in the $CH_3-Zr-CH_3A^-$ plane). Around the insertion transition state, the counteranion moves slightly further from the zirconium center (ca. 4.2 Å). After that, the anion reassociates to the zirconium again to form a bridged ion pair in a time period that takes less than 1 ps.

Solvation-Corrected FEP. The solvation-corrected FEPs are displayed in Figure 7A (dashed line). The solvation reduces the energy of TS1 by 4.0 kcal/mol, that of the π-complex by 5.0 kcal/mol, and that of TS2 by 5.1 kcal/mol, respectively. The *trans* approach is seen to have a larger solvent stabilization of TS1 in comparison to the cis approach, due to a large ion-pair separation.

3.3.2. The Second Insertion Step. As can be seen from the above discussion, the counteranion will recoordinate to the metal center completely and quickly to form the bridged ion pair $[Cp_2ZrPr]^+[CH_3A]^-$ after the first insertion step. The ethylene monomer has to displace the counteranion in the next step. Accordingly, we chose the bridged ion pair $[Cp_2ZrPr]^+[CH_3A]^-$

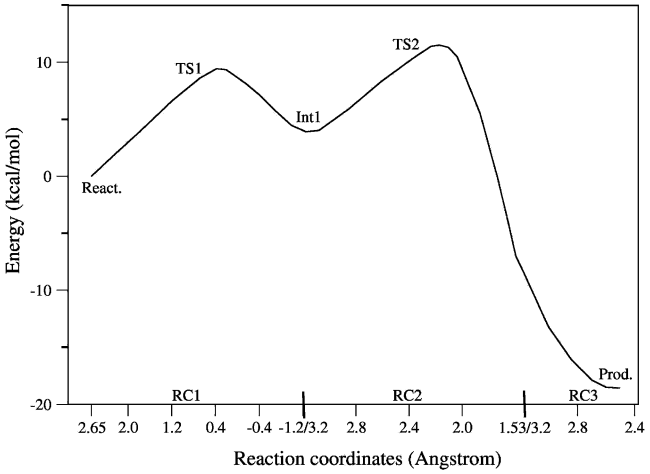

Figure 8. Potential energy profiles for the ethylene uptake, insertion, and ion-pair recombination in the cis path of the second insertion step.

as the resting state in the second step. It should also serve as a good model for a general propagation step as the polymer grows further. The same reaction coordinates (RC1, RC2, and RC3) used in the first insertion step were adopted again in the second step.

a. *cis* Approach. Potential Energy Profile. The calculated potential energy profiles along the reaction coordinates RC1, RC2, and RC3 are displayed in Figure 8. In comparison to the *cis* approach in the first insertion step, the ethylene uptake affords a higher barrier by 3.6 kcal/mol (Table 1), due to the increased steric congestion introduced by the propyl chain. The distances for Zr−X and Zr−C_A are 3.25 and 2.99 Å, which indicates that the ion-pair bridge is almost broken with the ethylene approaching the metal center. The ethylene π-complex is finally formed, with the counteranion further displaced by ethylene. The longer Zr−C_A distance (3.96 Å) in the π-complex indicates that the ion-pair bridge is completely broken. The π-complex has the ethylene double bond perpendicular to the equatorial plane. However, the C−C bond vector rotates to the equatorial plane to facilitate the ethylene insertion as TS2 is reached. In the insertion transition state (TS2), the ion pair is further separated due to the steric congestion in the equatorial plane induced by the ethylene rotation. The insertion barrier is 12.5 kcal/mol.

Free Energy Profile at 300 K. The calculated free energy profiles for the ethylene uptake, insertion, and ion-pair recombination are displayed in Figure 10A. In comparison to the PEP, the barriers of ethylene uptake and insertion in free energy increase by 8.2 and 11.6 kcal/mol, respectively. Also, the well corresponding to the π-complex is slightly deeper on the FEP compared to that on PEP.

The distance changes of Zr−C_A and the dihedral angle variations of C_E−X−Zr−C_α along RC1 and RC2 obtained from slow growth simulations are given in parts B and C of Figure 10, respectively. Starting from the left in Figure 10, the counteranion moves away as ethylene approaches the metal center. Near the uptake transition state (TS1), the Zr−C_A distance exhibits a sudden jump from 2.8 to 3.4 Å, which indicates that the ion-pair bridge is breaking up. In the ethylene π-complex, the average distance of Zr−C_A is 3.4 Å. Figure 10C shows that the dihedral angle C_E−X−Zr−C_α turns into ca. −90° in the π-complex, which implies that the ethylene approaches the catalyst in a perpendicular fashion. Starting from the π-complex, ethylene begins to rotate toward the α-carbon of alkyl (see Figure 10C). Meantime, the counteranion experiences

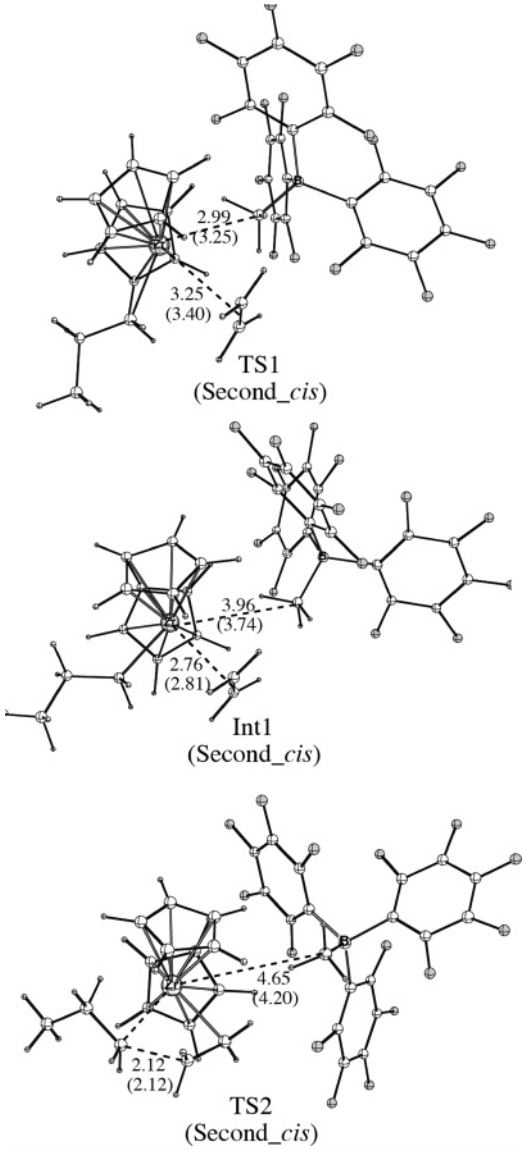

Figure 9. Calculated structures and selected bond distances for the transition state of ethylene uptake (TS1), ethylene π-complex (Int1), and insertion transition state (TS2) in the cis path of the second insertion step at 0 K (values in parentheses are the averaged bond distances at 300 K). Distances are given in Å.

considerable fluctuation in the Zr−C_A distance due to the steric congestion induced by the ethylene rotation. At the position of TS2 the total free energy barrier is 24.1 kcal/mol and Zr−C_A has reached a value of 3.2 Å. Starting from TS2 with Zr−C_A = 3.2 Å, another simulation without any constraint was conducted. The simulation demonstrated that the ion pair will recombine in a period of ca. 0.8 ps.

Solvation-Corrected FEP. The solvation-corrected FEP is displayed in Figure 10A. The solvation stabilizes the insertion transition state by ca. 6.9 kcal/mol and reduces the energy of the TS1 and π-complex by 1.5 and 4.5 kcal/mol, respectively.

b. *trans* Approach. Potential Energy Profiles. The potential energy profiles for the *trans* mechanism, where the ethylene approaches the catalyst *trans* to the counteranion, are displayed in Figure 11. Clearly, the PEP has a shape very similar to that in the first insertion step (see Figure 5). Again the PEP has a very flat area between TS1 and TS2, with a shallow well that represents the ethylene π-complex.

The calculated structures for TS1, Int1, and TS2 are shown in Figure 12. In the uptake transition state, the Zr−C_A distance

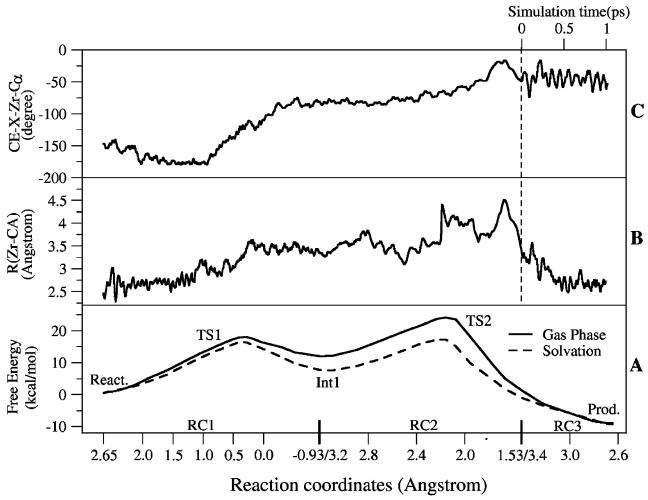

Figure 10. (A) Free energy profiles (300 K) for the ethylene uptake, insertion and ion-pair recombination in the cis path of the second insertion step. (B) $Zr-C_A$ distance changes along the reaction coordinates of RC1 and RC2. The right part of the dashed line gives the $Zr-C_A$ distance changes in the dynamic simulation without any constraint. (C) Dihedral angle $C_E-X-Zr-C_\alpha$ variations along the reaction coordinates of RC1 and RC2. The right part of the dashed line gives the dihedral angle $C_E-X-Zr-C_\alpha$ variations in the dynamic simulation without any constraint.

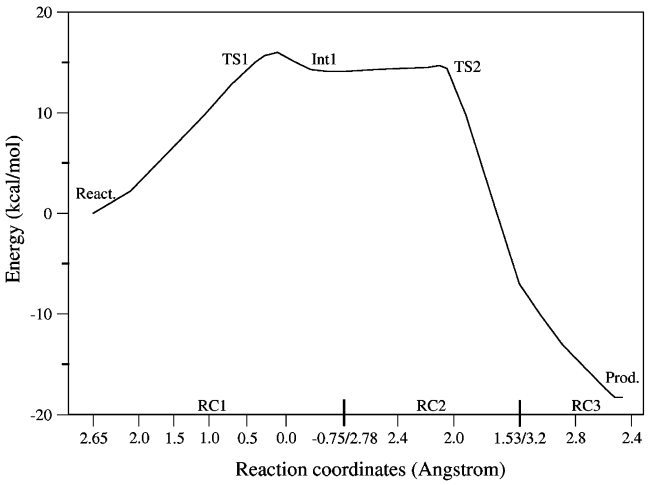

Figure 11. Potential energy profiles for the ethylene uptake, insertion, and ion-pair recombination in the trans path of the second insertion step.

is 3.42 Å, which indicates that the ion-pair bridge has been fully broken. This is due to the fact that the ethylene uptake by the metal center in an "in-plane" fashion introduces increasing steric congestion. In the π-complex, the ion pair is further separated to 3.5 Å. Again, this does not increase the energy of the π-complex due to the π-interaction between ethylene and zirconium. In the insertion transition state, the $Zr-C_A$ distance is further elongated to 3.78 Å. Nevertheless, the total energy has not been increased too much. A possible interpretation is that the reorientation of the counteranion, which can be seen in Figure 12, benefits the Coulombic interaction between the cation and the anion.

Free Energy Profile at 300 K. The calculated FEPs are depicted in Figure 13A. In comparison to the PEP, a clear well can be found on the FEP. The free energy barriers of ethylene uptake and insertion increase to 20.5 and 24.8 kcal/mol, respectively, due to entropy.

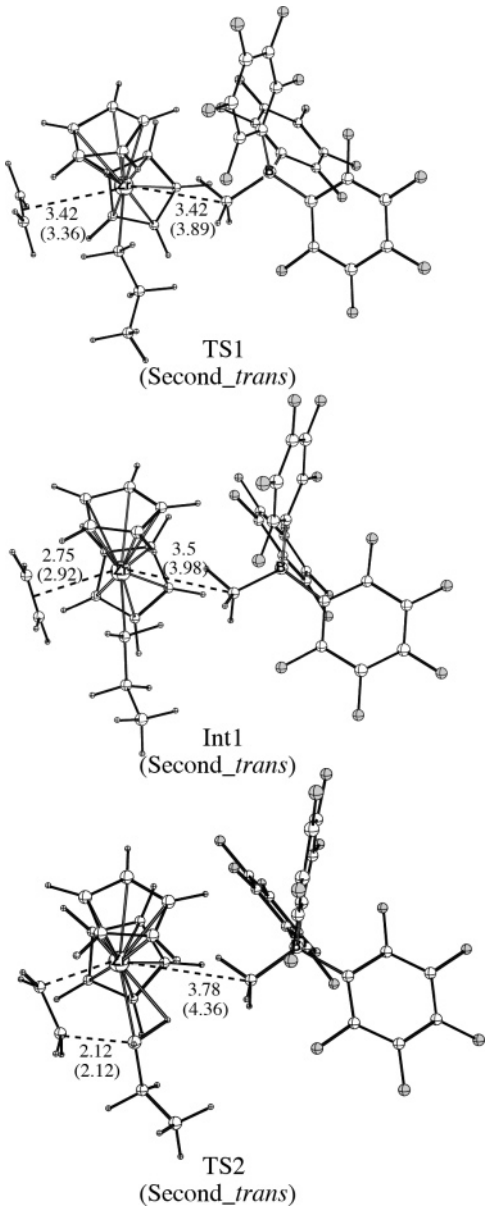

Figure 12. Calculated structures and selected bond distances for the transition state of ethylene uptake (TS1), ethylene π-complex (Int1), and insertion transition state (TS2) in the trans path of the second insertion step at 0 K (values in parentheses are the averaged bond distances at 300 K). Distances are given in Å.

The motion of the counteranion in the processes of ethylene uptake and insertion can be seen from the distance changes of $Zr-C_A$ along the reaction coordinates RC1 and RC2 (Figure 13B). Further, Figure 13C displays the torsion angle variation of $C_E-X-Zr-C_A$. Starting from the left in Figure 13, the counteranion departs as the ethylene approaches the metal center. In the ethylene π-complex, the average distance of $Zr-C_A$ is ca. 3.98 Å. The dihedral angle $C_E-X-Zr-C_A$ changes from 30° in the beginning to ca. −10° at the π-complex, which indicates that the ethylene directly enters the catalyst in an "in-plane" fashion. After the π-complex formation, the ethylene moves close to the α-carbon of the propyl and starts to insert into the $Zr-C_\alpha$ bond. In the insertion transition state (TS2), the $Zr-C_A$ distance is 4.36 Å. As it passes through TS2, the counteranion starts to recombine to the metal center. However, the distance for $Zr-C_A$ is still about 4 Å at the end of ethylene insertion, which indicates that the ion pair is still nonbridged. Starting from this point, another simulation without any

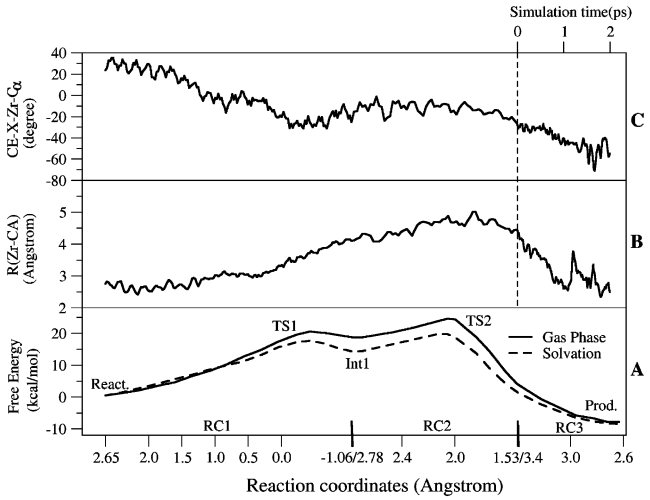

Figure 13. (A) Free energy profiles (300 K) for the ethylene uptake, insertion, and ion-pair recombination in the trans path of the second insertion step. (B) $Zr-C_A$ distance changes along the reaction coordinates of RC1 and RC2. The right part of the dashed line gives the $Zr-C_A$ distance changes in the dynamic simulation without any constraint. (C) Dihedral angle $C_E-X-Zr-C_\alpha$ variations along the reaction coordinates of RC1 and RC2. The right part of the dashed line gives the dihedral angle $C_E-X-Zr-C_\alpha$ variations in the dynamic simulation without any constraint.

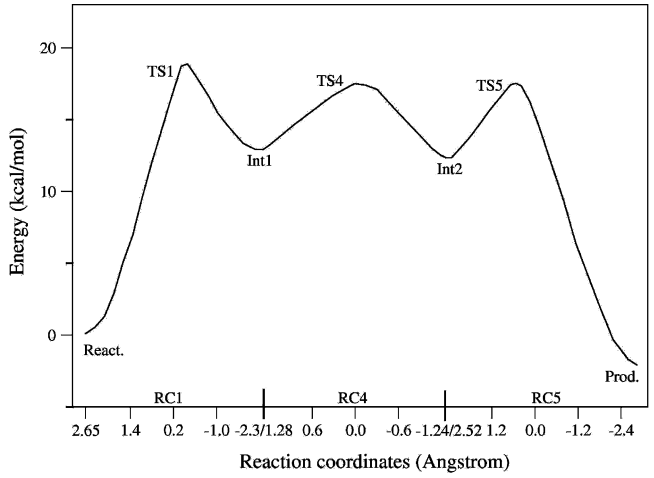

Figure 14. Potential energy profiles for the ethylene uptake, hydrogen transfer, and displacement of the propene by counteranion in the cis termination step.

constraint was conducted. The simulation shows that the ion pair will recombine in a period that is less than 1 ps.

Solvation-Corrected FEP. The solvation-corrected FEPs are displayed in Figure 13A (dashed line). The solvation stabilizes the insertion transition state by ca. 5.2 kcal/mol and reduces TS1 and the π-complex by ca. 2.8 and 4.6 kcal/mol, respectively.

3.4. Possible Ethylene Insertion before Counteranion Recombination. As discussed above, the counteranion finally recombines with the metal center after the ethylene insertion. However, dynamical simulations show that the ion pair is still nonbridged in the final period of ethylene insertion. Therefore, it is possible that a new ethylene monomer attacks the metal center and inserts into the $Zr-C_\alpha$ bond prior to the recombination of the ion pair. To investigate this possibility, we calculated the free energy barriers for the ethylene uptake and insertion with the ion pair nonbridged, where the $Zr-C_A$ distance is constrained to be 3.4 Å. Approaches of ethylene both *cis* and *trans* to the counteranion were considered. The calculated free energy barriers for the ethylene uptake and insertion in the *cis* pathway are 12.1 and 17.0 kcal/mol, respectively. For the *trans* approach, the calculated free energy barriers are 11.8 and 14.8 kcal/mol for the uptake and insertion, respectively. Qualitatively, one can conclude that the ion-pair recombination should be faster than insertion of a new monomer with the counteranion displaced at $Zr-C_A = 3.4$ Å, since the recombination is a barrierless process, as discussed in section 3.2. Quantitatively, one can use the transition state theory to estimate the time frequency for insertion of a new monomer with $Zr-C_A$ fixed at 3.4 Å from the uptake and insertion barrier. The estimated time frequency for the ethylene insertion is on the order of 10^{-2} s. This indicates that the ethylene insertion process is much slower than the recombination of the ion pair, for which the estimated time is 10^{-12} s.

3.5. Chain Termination. There has over the years been some debate about the mechanism for chain termination; it now seems clear that the termination in most cases takes place by a mechanism involving transfer of hydrogen to the incoming monomer.[19,44] We shall in the following discuss this mechanism.

The approach of ethylene leads to the formation of a π-complex, as discussed before. Starting from the π-complex, in addition to the further enchainment by ethylene insertion into the Zr−C bond, it is also possible for the polymer chain to terminate through the transfer of one hydrogen from the β-carbon of the chain to one ethylene carbon. The most energetically favorable pathways involve conformers of the π-complex with a β-hydrogen close to ethylene. Therefore, the conformers with a β-agostic hydrogen were chosen as the initial structures for the chain termination. Both the *cis* and *trans* approaches will be discussed.

The whole chain termination process is considered to consist of ethylene uptake, hydrogen transfer, and displacement of the generated propene by the counteranion. Three different reaction coordinates, RC1, RC4, and RC5 (introduced already in Scheme 1), were used to describe the three phases, respectively.

a. *cis* Approach. Potential Energy Profile. The three reaction coordinates vary from 2.65 to −2.3 for RC1, from 1.28 to −1.28 for RC4, and from 2.52 to −2.65 for RC5, respectively. The calculated potential energy profiles are displayed in Figure 14. Table 2 gives the relative energies for the reactant, intermediates, transition states, and product. From the PEP, one can find three peaks, which correspond to the transition states of the ethylene uptake (TS1), hydrogen transfer (TS4), and the

Table 2. Calculated Relative Energies (kcal/mol) for the Reactant, Ethylene Uptake Transition State (TS1), Ethylene π-Complex (Int1), Hydrogen Transfer Transition State (TS4), Propene π-Complex (Int2), Counteranion Recombination Transition State (TS5), and Product in the Termination Step

		reactant	TS1	Int1	TS4	Int2	TS5	product
cis	potential energy in gas phase (0 K)	0.0	18.9	12.9	16.3	12.2	17.5	−2.1
	free energy in gas phase (300 K)	0.0	21.0	17.2	24.8	19.8	24.2	−2.5
	free energy with solvation (300 K)	0.0	17.1	12.7	18.5	12.1	17.7	−4.0
trans	potential energy in gas phase (0 K)	0.0	17.5	15.6	21.7	9.7	12.2	−0.2
	free energy in gas phase (300 K)	0.0	19.8	17.8	25.6	11.9	20.8	−0.3
	free energy with solvation (300 K)	0.0	14.2	10.0	19.3	5.4	15.0	−2.4

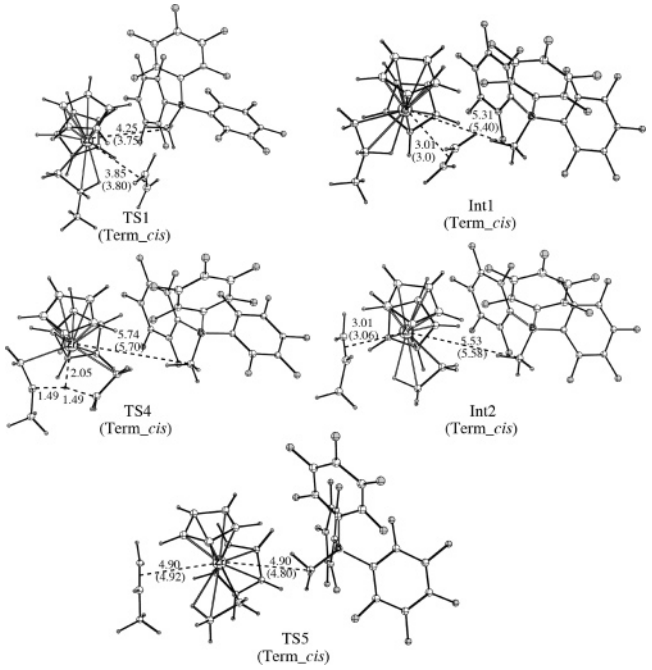

Figure 15. Calculated structures and selected bond distances for the transition state of ethylene uptake (TS1), ethylene π-complex (Int1), transition state of hydrogen transfer (TS4), propene π-complex (Int2), and transition state of displacement of the propene by counteranion (TS5) in the cis termination step at 0 K (values in parentheses are the averaged bond distances at 300 K). Distances are given in Å.

displacement of the generated propene by the counteranion (TS5). Two minima on the PEP correspond to the ethylene π-complex (Int1) and the propene π-complex (Int2). Ethylene uptake passes over a barrier of 18.9 kcal/mol, which compares well with the barrier of 15.0 kcal/mol obtained by static DFT calculations.[19] The subsequent barrier for hydrogen transfer is 16.3 kcal/mol, which is also comparable with the value of 14.7 kcal/mol obtained by static DFT calculations.[19] The ion-pair recombination and the subsequent displacement of propene has a barrier of 17.5 kcal/mol.

The calculated geometries and selected bond distances of the three transition states and two intermediates are displayed in Figure 15. In the transition state for ethylene uptake, the Zr−C_A distance is 4.25 Å, which means that the ion pair is fully separated. The early separation of the ion pair is due to the existence of a β-agostic bond, which occupies the coordinate space instead. The π-complex that is formed has the ion pair separated by 5.31 Å. In the transition state for hydrogen transfer, the Zr−C_A distance has been elongated slightly to 5.74 Å. After the hydrogen transfer, the propene π-complex with the ion pair nonbridged is formed, followed by ion-pair recombination and propene ejection, for which the barrier is 17.5 kcal/mol.

300 K Free Energy Profile at the Gas Phase. The reaction coordinates used at 0 K were also employed at 300 K with slightly different ranges. Figure 16A displays the free energy profile at 300 K. The Zr−C_A distance changes along the reaction coordinates are shown in Figure 16B. The ethylene uptake affords a free energy barrier of 21.0 kcal/mol (see Table 2), which is 2.1 kcal/mol higher than the corresponding potential energy barrier. Again, the difference is due to entropy. The hydrogen transfer has a free energy barrier of 24.8 kcal/mol, which is 8.5 kcal/mol higher than on the PEP. The resulting

(44) Vanka, K. Ph.D. Thesis, University of Calgary, 2004.

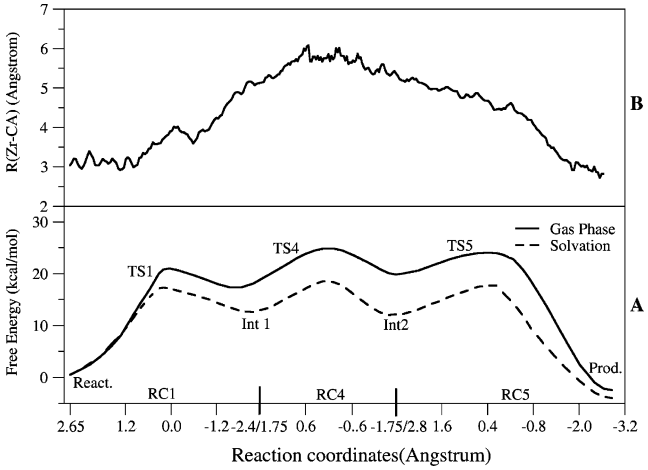

Figure 16. (A) Free energy profiles (300 K) for the ethylene uptake, hydrogen transfer, and displacement of the propene by the counteranion in the cis termination step. (B) Zr−C_A distance changes along the reaction coordinates of RC1, RC4, and RC5.

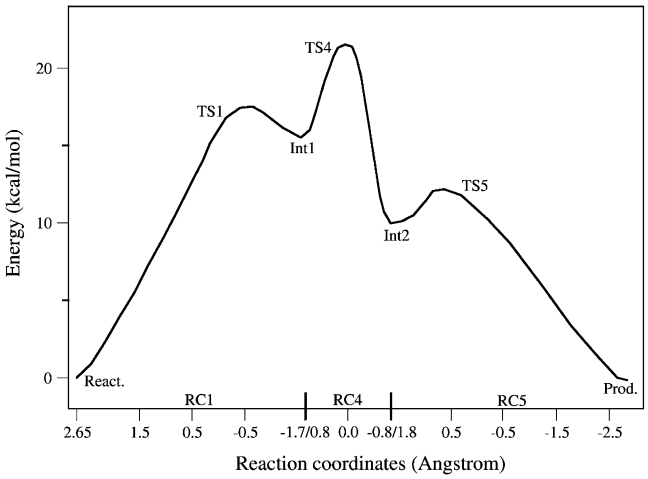

Figure 17. Potential energy profiles for the ethylene uptake, hydrogen transfer, and displacement of the propene by counteranion in the trans termination step.

propene π-complex (Int2) is slightly less stable than the ethylene π-complex (Int1) due to steric factors. The ion-pair recombination and concurrent displacement of the generated propene affords a free energy barrier of 24.2 kcal/mol, which is 6.7 kcal/mol higher than the corresponding energy barrier on the PEP.

Solvation-Corrected 300 K Free Energy Profile. The solvation-corrected free energy profiles are displayed in Figure 16A (dashed curve). Solvation decreases the barriers of ethylene uptake and hydrogen transfer by ca. 4 and 6 kcal/mol, respectively, through a stabilization of the transition states TS1 and TS4. The greatest stabilization (6.5 kcal/mol) occurs in TS5, which is due to the large separation of the ion pair.

b. *trans* Approach. Potential Energy Profile. The calculated potential energy profiles are displayed in Figure 17. Figure 18 shows the calculated geometries and selected bond distances. The relative energies for the reactant, transition states, intermediates, and product are given in Table 2. There are three barriers on the PEP, which represent the transition states of ethylene uptake (TS1), hydrogen transfer (TS4), and displacement of the generated propene by the counteranion (TS5). Between the peaks, there are two intermediates on the PEP, corresponding to the ethylene π-complex (Int1) and propene π-complex (Int2), respectively. The ethylene uptake barrier is 17.5 kcal/mol, comparable with a value of 17.0 kcal/mol from

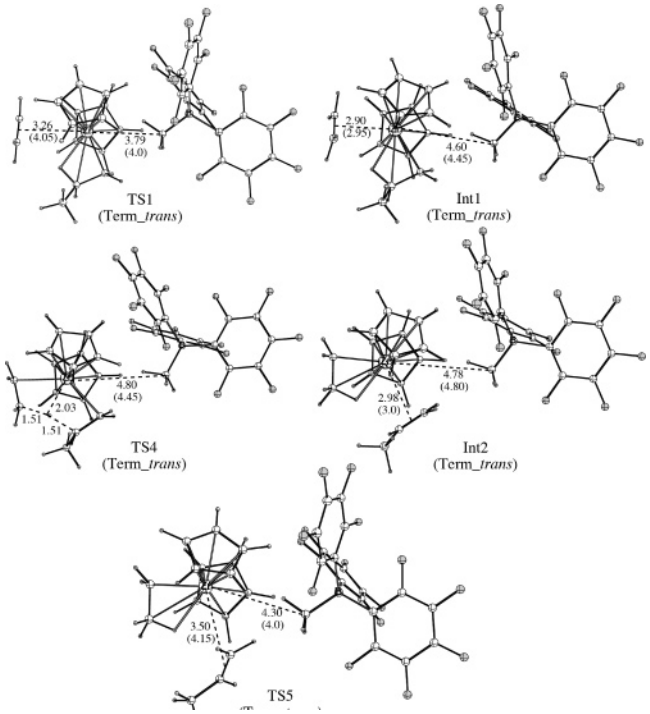

Figure 18. Calculated structures and selected bond distances for the transition state of ethylene uptake (TS1), ethylene π-complex (Int1), transition state of hydrogen transfer (TS4), propene π-complex (Int2), and transition state of displacement of the propene by counteranion (TS5) in the trans termination step at 0 K (values in parentheses are the averaged bond distances at 300 K). Distances are given in Å.

a static DFT calculation.[19] In the transition state of ethylene uptake, the distances of Zr−X and Zr−C_A are 3.26 and 3.79 Å, respectively, which indicates that the ion pair has been separated already at this stage. In the ethylene π-complex that is formed, the ion pair is further separated to 4.60 Å. The transition state of hydrogen transfer, where the Zr−C_A distance is 4.80 Å, affords a barrier of 21.7 kcal/mol. The generated propene π-complex with the propene *cis* to the counteranion has an energy of 9.7 kcal/mol. The Zr−C_A distance is 4.78 Å. Finally, the propene is displaced by the counteranion, passing a barrier of 12.2 kcal/mol.

300 K Free Energy Profile in the Gas Phase. The dynamics simulations with the reaction coordinates constrained were conducted to calculate the free energy profile, which has been depicted in Figure 19A. Figure 19B gives the Zr−C_A distance obtained from a slow growth simulation. The ethylene uptake has a free energy barrier of 19.8 kcal/mol, which is just 2.3 kcal/mol higher than the potential energy barrier (see Table 2). This small change between the barriers on the PEP and the FEP is not surprising if one considers the structure of TS1. In TS1, the Zr−C_A distance is about 4.0 Å, which indicates that the ion pair has been separated already (see Figure 19B). This separation helps to compensate for the reduction in entropy due to ethylene capture. The hydrogen transfer has a free energy barrier of 25.6 kcal/mol, which is higher by 3.9 kcal/mol over the corresponding potential energy barrier. The counteranion reassociation to the metal center and propene displacement affords a barrier of 20.8 kcal/mol, which is higher by 8.6 kcal/mol than the potential energy barrier.

Solvation-Corrected 300 K Free Energy Profile. The solvation-corrected free energy profile is displayed in Figure 19A (dashed curve). The solvation decreases the barriers of ethylene uptake, hydrogen transfer, and counteranion recombination by 5.6, 6.3, and 5.8 kcal/mol, respectively. Also, the intermediate ethylene and propene π-complexes are stabilized by 7.8 and 6.5 kcal/mol, respectively.

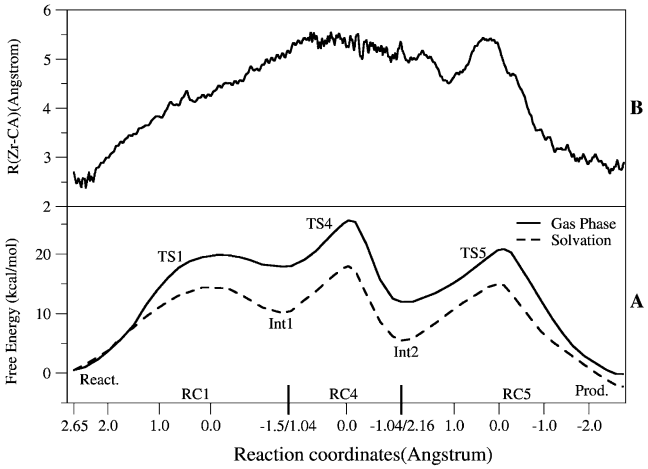

Figure 19. (A) Free energy profiles (300 K) for the ethylene uptake, hydrogen transfer, and displacement of the propene by counteranion in the trans termination step. (B) Zr−C_A distance changes along the reaction coordinates of RC1, RC4, and RC5.

3.6. Summary and Comparison with Experiment. The whole possible catalytic polymerization cycle, including the first and second insertion steps and chain termination with both *trans* and *cis* paths involved, has been modeled above. For the chain propagation, the calculated free energy profiles indicate that the *cis* pathway is preferred over the *trans* pathway for both the first and second insertion steps. Also, the ethylene insertion into the Zr−C_α bond, rather than the ethylene uptake by the metal center, is the rate-determining step. The free energy favorable pathway, which affords a free energy barrier of 17.2 kcal/mol, corresponds to the *cis* path in the second insertion step. For the chain termination step, the *cis* pathway (free energy barrier 18.5 kcal/mol) is favored over the *trans* pathway.

A very recent experimental reaction kinetic investigation on a similar zirconocene (*rac*-$(C_2H_4(1\text{-indenyl})_2)Zr(MeB(C_6F_5)_3)$-polymeryl) reported the observed rate constants for the chain propagation (0.0012 M^{-1} s^{-1})[45] and termination (0.0002 s^{-1}). On the basis of the transition state theory, the estimated free energy barriers are 16.6 and 17.5 kcal/mol for the chain propagation and termination, respectively. This clearly indicates that our theoretical results are consistent with the experimental results.

4. Concluding Remarks

Combined quantum mechanics and molecular mechanics (QM/MM) dynamic simulations have been performed to investigate the polymer chain propagation and termination processes in the ethylene polymerization catalyzed by zirconocene with the counteranion $[CH_3B(C_6F_5)_3]^-$ involved. The simulation results allow us to draw the following conclusions.

(1) The initial catalyst activated by the Lewis acid $B(C_6F_5)_3$ can best be described as a $Zr(\mu\text{-}CH_3)B(C_6F_5)_3$ bridged ion pair. The dissociation of the ion pair is a thermodynamically uphill process without a kinetic barrier, both on the potential energy surface and on the free energy surface. The nonbridged ion pair prefers to adopt an orientation where the methyl group in the

(45) The original paper gives two rate constants: i.e., "initiation" and "propagation". However, only the "initiation" corresponds to the propagation defined here.

counteranion $[CH_3B(C_6F_5)_3]^-$ is oriented along the alkyl chain in order to minimize steric interaction.

(2) For the chain propagation, the FEPs differ from the PEPs in the barrier height and the shape. In general, the FEPs give higher free energy barriers by 5−14 kcal/mol over the corresponding potential energy barriers on the PEPs. The transition state of ethylene uptake to the metal center, π-complex, and ethylene insertion transition state are clearly present on the FEPs. This is not always the case on the PEPs, especially for the trans pathway. The calculated FEPs for the chain propagation indicate that the *cis* pathway is preferred over the *trans* pathway for both the first and second insertion steps. For the energetically favorable *cis* pathway, ethylene insertion into the $Zr-C_\alpha$ bond rather than ethylene uptake by the metal center is the rate-determining step on both the PEP and the FEP (with/without solvation effects included).

(3) The PEPs and FEPs were also calculated for the polymer chain termination achieved by a β-hydrogen transfer from the β-carbon on the polymer chain to one carbon of the entering ethylene monomer. Our calculations show that the *cis* pathway, which affords a barrier of 18.5 kcal/mol, is favored over the *trans* pathway.

(4) Free dynamic simulations without any constraint after the ethylene insertion show that the ion pair can recombine in a period of less than 1 ps. In comparison with the estimated time scale of the chain propagation, the counteranion, which was displaced by ethylene in the ethylene uptake process, has sufficient time to recombine to the metal center again before the new monomer approaches the metal center. This is in good agreement with a recent experiment.[14]

Acknowledgment. An important part of the calculations was performed on the Westgrid cluster of Canada. This work has been supported by the National Sciences and Engineering Research Council of Canada (NSERC). T.Z. thanks the Canadian government for a Canada Research Chair.

OM050840S